Dynamical Adjustment of the Trade Wind Inversion Layer

WAYNE H. SCHUBERT, PAUL E. CIESIELSKI, CHUNGU LU, AND RICHARD H. JOHNSON

Department of Atmospheric Science, Colorado State University, Fort Collins, Colorado

(Manuscript received 8 July 1994, in final form 14 February 1995)

ABSTRACT

In schematic north–south cross sections the trade inversion layer is often depicted as sloping upward as air flows toward the intertropical convergence zone. This conceptual view is consistent with *purely thermodynamic* boundary-layer models, which predict a deeper boundary layer with increasing sea surface temperature and decreasing large-scale subsidence. The slopes implied by such thermodynamic models and incorporated into schematic diagrams are approximately 2000 m/1000 km. In contrast, observational studies of the inversion structure over the Atlantic and Pacific Oceans reveal a less dramatic slope, on the order of 300 m/1000 km. To address this inconsistency, the authors adopt a somewhat different view of the trade inversion layer. In particular, rather than regarding it as a purely thermodynamic structure, it is regarded as a dynamical structure. By formulating a generalization of the Rossby adjustment problem, the authors investigate the dynamical adjustments of a trade wind inversion layer of variable strength and depth. From the solution of the adjustment problem, there emerges the notion that the subtropics control the inversion structure in the Tropics; that is, the subtropical inversion height is dynamically extended into the Tropics in such a way that there is little variation in the depth of the boundary layer.

1. Introduction

Most of the latent heat release and rising motion of the tropical atmosphere occurs in the intertropical convergence zone (ITCZ) and its associated wave disturbances. The area involved in this rising motion is a small percentage of the total area of the Tropics. Most of the tropical–subtropical region is under the influence of subsidence. In the subsidence regions stratocumulus and shallow cumulus convection is capped by the stable trade wind inversion[1] layer. For example, at the subtropical station Porto Santo, in the Madeira Islands (33.1°N, 16.3°W), where the cloudiness is a mixture of stratocumulus and shallow cumulus, the statistics of the trade inversion are as shown in Fig. 1. This figure is based on 203 high vertical resolution (10–15 m) radiosonde soundings (Schubert et al. 1992) taken between 1 and 28 June 1992. At each level for each sounding, the lapse rate $\partial T/\partial z$ was calculated using a centered vertical difference. At a particular level, the percentage of observations falling into each 1 K km^{-1} sized lapse rate bin was then calculated. This frequency distribution was then contoured, as shown in Fig. 1a. Three cumulative frequency distributions were then calculated (Fig. 1b) for lapse rates greater than −4.0, 0.0, and 4.0 K km^{-1}, respectively. These diagrams indicate that the most probable trade inversion height at Porto Santo is slightly below the 800-mb (≈2000 m) level, with a tendency for the stronger inversions to be somewhat lower and near 850 mb (≈1500 m).

For comparison, the same analysis was performed on 70 high-resolution radiosonde soundings (Schubert et al. 1987) taken between 30 June and 20 July 1987 at San Nicolas Island, California (33.3°N, 119.6°W). The results of this analysis are shown in Fig. 2. At San Nicolas the sea surface is colder and the mean divergence is larger than at Porto Santo, resulting in a persistent stratocumulus regime rather than the mixed stratocumulus/shallow cumulus regime observed at Porto Santo. Note that the inversions at San Nicolas tend to be lower and stronger than those at Porto Santo. For example, at San Nicolas the highest probability of strong inversions ($\partial T/\partial z > 4.0$ K km^{-1}) occurs at 915 mb (≈850 m) and is 24%, while at Porto Santo the highest probability of strong inversions occurs at 860 mb (≈1400 m) and is 15%.

Evidence concerning the large-scale structure of the trade wind boundary layer has been slowly accumulating for much of this century. Some of the earliest data were acquired from the 1925–27 expedition of the German R/V *Meteor I*. During this expedition, 217 kite soundings of the Atlantic trade wind boundary layer were obtained. Based on this data, von Ficker (1936)

[1] As is often done, we shall use the term "inversion" in a generic sense to include not only layers in which $\partial T/\partial z > 0$ but also layers of enhanced stability in which $\partial T/\partial z$ is slightly negative.

Corresponding author address: Dr. Wayne H. Schubert, Department of Atmospheric Science, Colorado State University, Fort Collins, CO 80523-1371

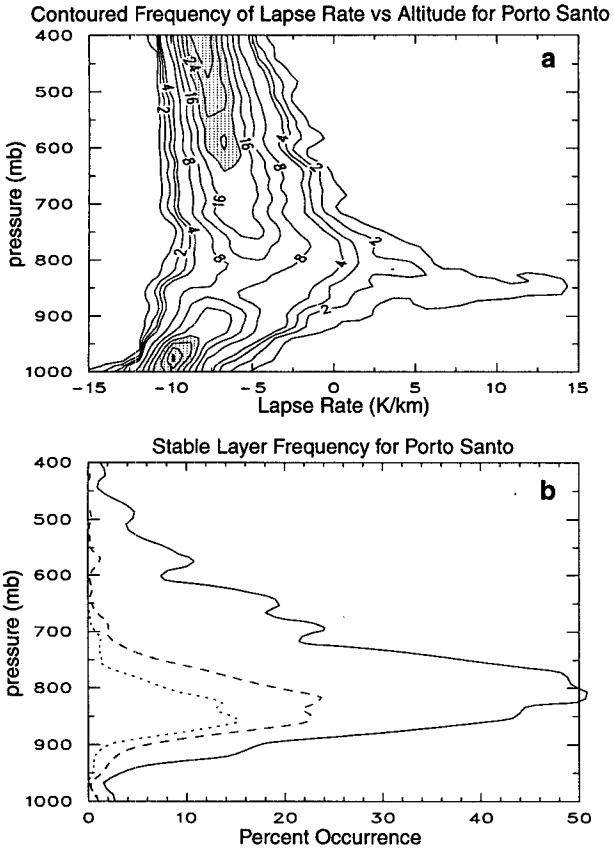

FIG. 1. Sounding statistics for 203 high resolution radiosonde soundings at Porto Santo Island (33.1°N, 16.3°W) from 1 to 28 June 1992. (a) Isolines of the frequency (percent) of observations, at a particular level, which have lapse rates in a 1 K km^{-1} size bin; note that the contour interval is 1% for low frequencies and 4% for frequencies higher than 4%. (b) Cumulative frequency (percent) of lapse rates greater than −4 K km^{-1} (solid curve), 0 K km^{-1} (dashed curve), and 4 K km^{-1} (dotted curve).

produced the first map of the height of the trade wind inversion base over the Atlantic (Fig. 3). The map, which can be regarded as typical of the northern summer, shows low inversions over the cold ocean currents near northwest and southwest Africa. These two regions of low inversions are similar in many respects to San Nicolas Island. Figure 3 also shows a fairly flat inversion at approximately 2000 m over much of the equatorial region. Later Atlantic observations, analyzed by Augstein et al. (1974), Holland and Rasmusson (1973), and Nitta and Esbensen (1974), support the general picture given by von Ficker.

Gutnick (1958) extended the study of the trade wind inversion into the Caribbean by analyzing three years of radiosonde soundings for six stations (approximately 3800 total soundings). We have prepared a map of the height of the trade wind inversion base (Fig. 4) for April based on the tabular data presented by Gutnick. This map reveals a trade wind inversion base at approximately 2200 m over the Caribbean, with a gentle upward slope (≈250 m/1000 km) toward the equator.

A depiction of the trade wind inversion structure over the tropical eastern Pacific was provided by Firestone and Albrecht (1986) and Betts and Albrecht (1987), who analyzed dropwindsonde data from approximately 900 soundings made on flights between Hawaii and the equator during the first special observing period (15 January–20 February 1979) of the First GARP Global Experiment (FGGE). The sondes produced soundings with approximately 4-mb vertical resolution between 200 mb and the surface. Based on these data, the mean north–south cross section reproduced in Fig. 5 was constructed. The solid lines are isolines of saturation equivalent potential temperature, and the dashed line indicates the inversion height based on the minimum saturation equivalent potential temperature. An important conclusion of this work was that there is only a slight increase in the height of the trade inversion (≈300 m/1000 km) toward the equator over the eastern Pacific.

In an extension of the previous two studies, Kloesel and Albrecht (1989) analyzed additional dropwind-

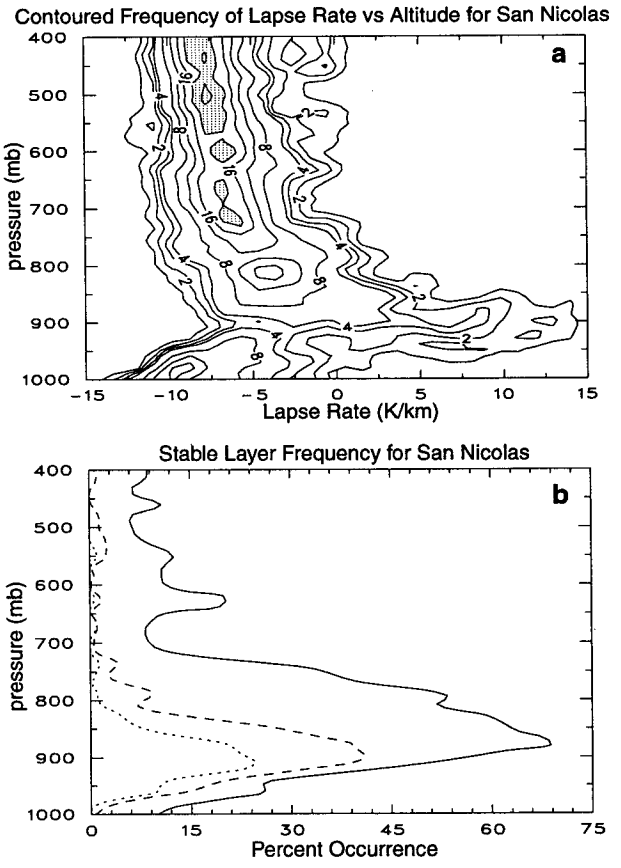

FIG. 2. Sounding statistics for 70 high-resolution radiosonde soundings at San Nicolas Island (33.3°N, 119.6°W) from 30 June to 20 July 1987 in a format identical to Fig. 1.

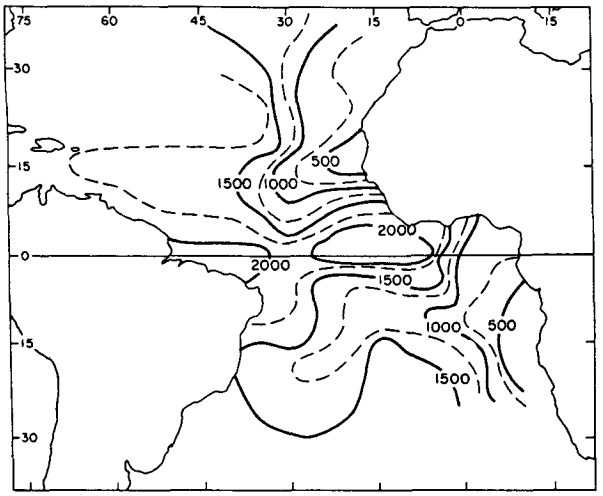

FIG. 3. Height (m) of the base of the trade wind inversion over the Atlantic, as determined from data obtained during the 1925–27 *Meteor I* expedition (von Ficker 1936).

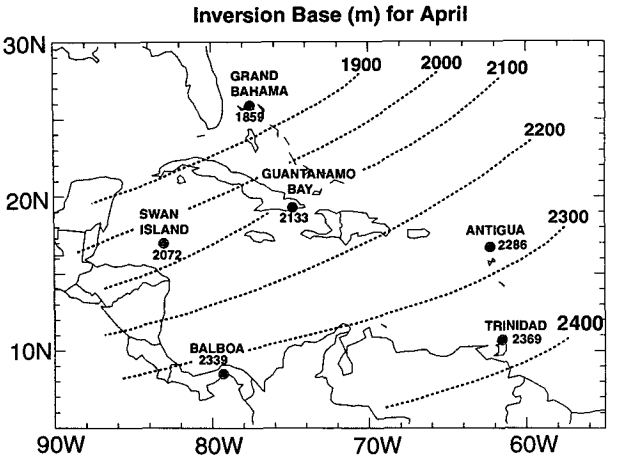

FIG. 4. Height (m) of the base of the trade wind inversion over the Caribbean for April. The map is based on the tabular data of Gutnick (1958).

sonde soundings made on flights south of Acapulco and southwest of the Panama Canal Zone during the second special observing period (10 May–8 June 1979) of FGGE. Based on this extended dataset, Kloesel and Albrecht concluded that the trade inversion height is uniform over the entire tropical eastern Pacific from 5°S to 15°N and from 90°W to 170°E. These results from dropwindsonde sounding studies are consistent with the aircraft-sounding study of Ramage et al. (1981), who analyzed National Oceanic and Atmospheric Administration P3 aircraft data taken on flights between Hawaii and Tahiti. The low inversion heights evident in the dropsonde data are also consistent with ship-based radiosonde measurements of Chertock et al. (1993) made at 0°N, 140°W during November and December 1991. These data reveal an average trade inversion height of 1685 m, determined from 46 soundings.

In a preliminary analysis of Tropical Ocean Global Atmosphere (TOGA) Coupled Ocean–Atmosphere Response Experiment (COARE) sounding data, Johnson et al. (1993) have provided evidence that trade wind inversion heights over the western Pacific tend to be horizontally uniform and near 800 mb, just as in the eastern Pacific and in the Atlantic. As further evidence, Fig. 6 shows the results of a statistical analysis of soundings taken at Kwajelein Atoll in the Marshall Islands (8.7°N, 167.7°E) during November 1992–February 1993. The lapse rate statistics for Kwajelein are similar to those at Porto Santo (Fig. 1), with a most probable inversion height of 800 mb. Also apparent in the Kwajelein statistics is a secondary region with a high frequency of stable layers located between 550 and 600 mb. Johnson et al. (1995) have pointed out that soundings taken in the tropical western Pacific warm pool region reveal the common occurrence of thin stable layers near the 0°C level (~560 mb). These features, which are also apparent in the work of Haraguchi (1968), are extensively analysed by Johnson et al. (1995), who associate them directly and indirectly with the melting process within stratiform rain regions.

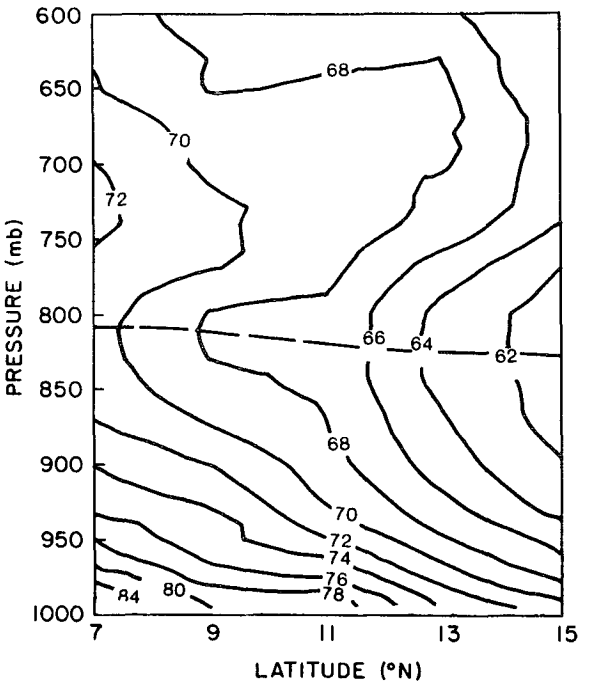

FIG. 5. Mean north–south cross section of saturation equivalent potential temperature (C°) near 165°W, based on dropwindsonde soundings taken between 15 January and 20 February 1979. The dashed curve indicates the inversion height based on the minimum saturation equivalent potential temperature. (Firestone and Albrecht 1986).

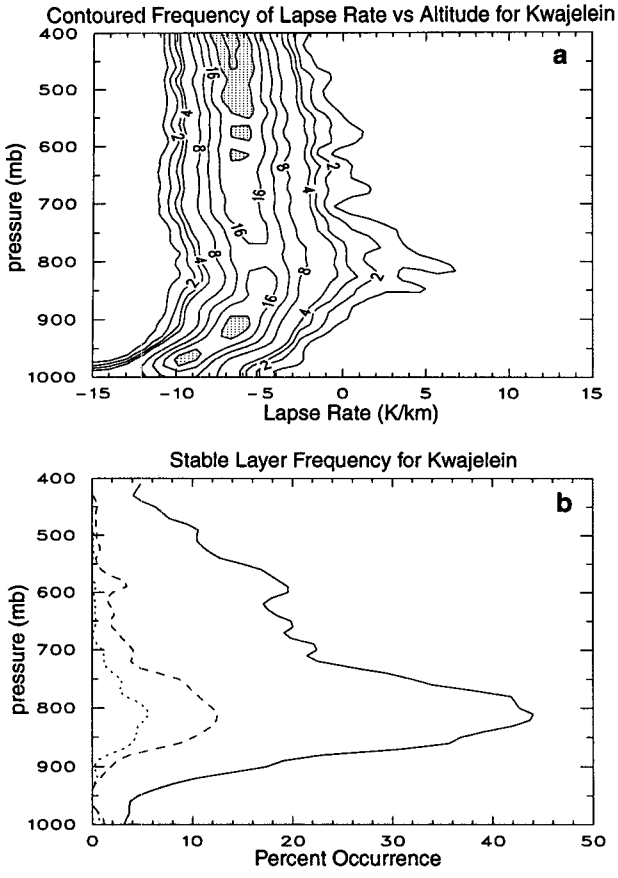

FIG. 6. Sounding statistics for 252 high-resolution radiosonde soundings at Kwajelein (8.7°N, 167.7°E) from 1 November 1992 to 28 February 1993 in a format identical to Fig. 1.

Since these higher-level inversions seem to be physically distinct from the lower-level trade inversions, we shall not discuss them here.

Two theoretical views of the trade inversion are as follows: The first (e.g., Lilly 1968; Betts 1973; Schubert et al. 1979a; Albrecht et al. 1979; Albrecht 1979; Randall 1980; Sarachik 1985; Bretherton 1993) considers the trade inversion as a pure thermodynamical phenomenon that can be modeled using steady-state, horizontally homogeneous assumptions. In such one-dimensional thermodynamic models of stratocumulus and shallow cumulus, the equilibrium trade wind boundary-layer depth is determined by a balance between the radiative and moist convective processes tending to deepen the layer and the large-scale subsidence tending to shallow the layer. This view leads to the notion that the boundary-layer depth and thermodynamic structure are controlled by local values of sea surface temperature and large-scale divergence. The second view (e.g., Schubert et al. 1979b; Wakefield and Schubert 1981; Albrecht 1984) also involves pure thermodynamical, steady-state arguments but recognizes the importance of horizontal inhomogeneities. In this view, horizontal advection is important, and entrainment can occur not only by large-scale subsidence but also by horizontal flow across a sloping inversion. This view leads to the notion that the boundary-layer depth and thermodynamic structure are controlled by a weighted average of the sea surface temperature and large-scale divergence upstream along the trajectory. Both of these views predict a deepening boundary layer along trajectories moving toward the ITCZ over increasing sea surface temperature and decreasing large-scale subsidence. In possession of concepts like these, it is natural to construct schematic cross sections such as that shown in Fig. 7a, which depicts the trade inversion as sloping upward from very near the sea surface in the subtropics to the midtroposphere near the edge of the ITCZ. The slopes implied by such thermodynamic models and incorporated into many existing schematic diagrams are approximately 2000 m/1000 km, in contrast to observed values of 300 m/1000 km. The observed values are more consistent with the schematic cross sections shown in Fig. 7b.

The solutions of the equilibrium thermodynamic models discussed above require specification of several external parameters, including the sea surface temperature and the large-scale subsidence. Although the sea surface temperature is well observed, the large-scale subsidence is not. The usual procedure is to specify climatological mean subsidence profiles, which show weakening large-scale subsidence on trajectories approaching the ITCZ. However, near the ITCZ deep convection may coexist with a weakened trade inversion structure, and cumulus-induced subsidence due to the deep convection may contribute to a lowering of the trade inversion height. According to this argument the equilibrium thermodynamic models may deepen the trade wind boundary layer too rapidly along trajectories approaching the ITCZ, simply because the specified subsidence is too weak. While there may be some merit to this argument, which requires further investigation, we shall pursue a different line of reasoning here. In an effort to understand why the observed trade wind inversion layer is so flat, we shall adopt a view that emphasizes the dynamical aspects of the problem and highlights the incompleteness of the pure thermodynamic models. In particular, although the thermodynamic models can easily produce sloped inversions in the Tropics, such sloping inversions imply large horizontal temperature gradients, which dynamical adjustment processes tend to flatten (e.g., Schneider 1977; Held and Hou 1980; Hack et al. 1989). In fact, we shall see that the inclusion of these dynamical adjustment processes puts constraints on both the slope and sharpness of the trade inversion.

Thus, let us consider the following problem. If thermodynamic processes tend to deepen the trade wind boundary layer toward the equator, will dynamical adjustment processes oppose this effect and restore a nearly flat trade wind inversion height? We can think

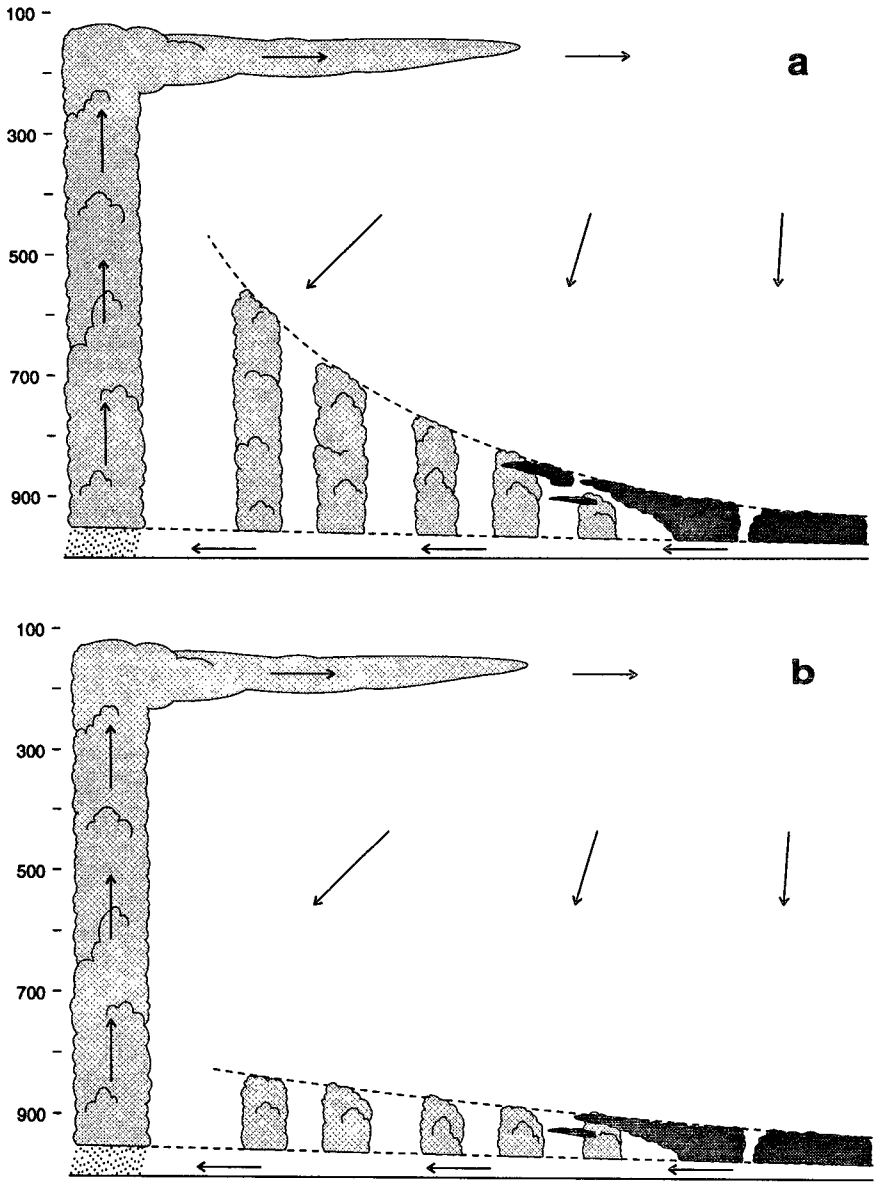

FIG. 7. Schematic north–south cross sections depicting two differing views of trade wind inversion structure. The cross sections cover an area from the subtropics (~30°N, on the right) to the ITCZ (~10°N, on the left). (a) A steeply sloped (~2000 m/1000 km) trade inversion rising from below 1000 m in the subtropics to the midtroposphere near the edge of the ITCZ. (b) In contrast, a gently sloped (~300 m/1000 km) trade inversion. The latter depiction is more consistent with observations.

of this as a generalized version of the classic Rossby adjustment problem. It is generalized in the sense that nonlinearity, continuous stratification, and the earth's sphericity are included. In section 2 we present the mathematical formulation of this problem using latitude and potential temperature as the independent spatial variables. In this formulation the potential vorticity principle is in the form of a material conservation relation that includes meridional advection. In section 3 we transform the problem using potential latitude and potential temperature as the independent spatial variables; this results in a potential vorticity principle with the form of a local conservation relation. This local conservation relation, coupled with an invertibility principle, allows us to directly compute the final balanced state from the initial unbalanced state, without computing the details of the intermediate transient states. In section 4 we present the results of idealized experiments that illustrate two concepts: the dynamical extension of subtropical inversions into the Tropics and

the dynamical adjustment of sloping trade wind inversion layers. Those readers not interested in the detailed mathematical analysis should skip directly to section 4.

2. Dynamical adjustment problem in the latitude coordinate

Let us begin by drawing an analogy between our adjustment problem and the classic Rossby shallow water adjustment problem on an f plane. The simplest way to solve for the final adjusted state in the linear Rossby adjustment problem for the shallow water equations on an f plane is as follows. First derive the potential vorticity principle, which turns out to be a *local* conservation relation, so that the final potential vorticity equals the initial potential vorticity point by point. Then assume the final flow is geostrophic and, hence, obtain a second-order differential equation for the final adjusted geopotential. The solution of this second-order equation gives us essentially everything we need, that is, the final wind and mass fields. Our trade inversion problem is more general in three respects: it is nonlinear; it is on the sphere rather than the f plane; and it is continuously stratified rather than shallow water. It is the nonlinear aspect that causes the most difficulty. How can we get a "local conservation relation" for the potential vorticity when the problem is nonlinear? In fact, this might appear impossible, because potential vorticity is *materially* conserved and hence must be advected. But, if we use the isentropic coordinate in the vertical and the potential latitude coordinate in the horizontal, we can get a local conservation relation. Then we simply express the invertibility principle in these same coordinates. The analogy with the linear, f-plane, shallow water, Rossby adjustment problem is complete, that is, one local conservation relation and an invertibility principle. But before presenting the formulation of our adjustment problem in the potential latitude coordinate (section 3), let us discuss its formulation in the ordinary latitude coordinate.

Consider the inviscid, adiabatic, zonally symmetric adjustments of a compressible, stably stratified quasi-static atmosphere on the sphere. Using the latitude ϕ as the horizontal coordinate and the potential temperature θ as the vertical coordinate, the quasi-static primitive equations for such flows can be written

$$\frac{Du}{Dt} - \left(2\Omega \sin\phi + \frac{u \tan\phi}{a}\right)v = 0, \tag{1}$$

$$\frac{Dv}{Dt} + \left(2\Omega \sin\phi + \frac{u \tan\phi}{a}\right)u + \frac{\partial M}{a\partial\phi} = 0, \tag{2}$$

$$\frac{\partial M}{\partial\theta} = \Pi, \tag{3}$$

$$\frac{D\sigma}{Dt} + \sigma \frac{\partial(v \cos\phi)}{a \cos\phi\, \partial\phi} = 0, \tag{4}$$

where

$$\frac{D}{Dt} = \frac{\partial}{\partial t} + v\frac{\partial}{a\partial\phi} \tag{5}$$

is the material derivative; u and v are the zonal and meridional components of the wind; $\Pi = c_p(p/p_0)^\kappa$, the Exner function; $M = \theta\Pi + gz$, the Montgomery potential; and $\sigma = -\partial p/\partial\theta$, the pseudodensity in θ-space. Using the definitions of Π and σ, the set (1)–(4) can be considered closed in the unknowns u, v, p, and M.

Assuming $z = 0$ on the isentropic bottom boundary $\theta = \theta_B$ and $p = p_T$ on the isobaric and isentropic top boundary $\theta = \theta_T$, the total energy principle, derived from (1)–(4), is $K + A =$ constant, where

$$K = \iint \tfrac{1}{2}(u^2 + v^2)\sigma a \cos\phi d\phi d\theta \tag{6}$$

is the kinetic energy and

$$A = \frac{p_0 c_p}{1+\kappa}\iint [(p/p_0)^{1+\kappa} - (\bar{p}/p_0)^{1+\kappa}]a \cos\phi d\phi d\theta \tag{7}$$

is the available potential energy, with the integrals in (6) and (7) extending from the South Pole to the North Pole and from θ_B to θ_T, and with $\bar{p}(\theta)$ denoting the average pressure on an isentropic surface [see (23)]. To account for situations in which isentropes intersect the earth's surface, extended definitions of p and $\bar{p}(\theta)$ are possible. With these extended definitions, isentropes intersecting the earth's surface are assumed to continue along the earth's surface with an assigned value of pressure equal to the surface pressure. The lower boundary potential temperature θ_B is then the largest θ that lies everywhere along the earth's surface.

If we specify an initial condition such that $v = 0$ and $(2\Omega \sin\phi + (u \tan\phi)/a)u + \partial M/a\partial\phi \neq 0$, then v will be generated through (2), and the rotational wind field u and the mass field σ will subsequently change through (1) and (4). As gravity–inertia waves propagate outward, the rotational flow will come into adjustment, and v will return to zero. This nonlinear adjustment process consists of two parts: the transient part and the final adjusted part. The final adjusted part of the problem can be treated using potential vorticity or potential pseudodensity conservation principles and is independent of the details of the transient part of the adjustment. Here we shall discuss only the final adjusted state.

The potential vorticity principle associated with the set (1)–(4) can be derived by first noting that the equation for the *isentropic absolute vorticity* takes the form

$$\frac{D\zeta}{Dt} + \zeta \frac{\partial(v \cos\phi)}{a \cos\phi\, \partial\phi} = 0, \tag{8}$$

where $\zeta = 2\Omega \sin\phi - \partial(u \cos\phi)/(a \cos\phi\, \partial\phi)$ is the isentropic absolute vorticity. Eliminating the isentropic divergence between (4) and (8) we obtain

$$\frac{DP}{Dt} = 0, \tag{9}$$

where $P = \zeta/\sigma$ is the potential vorticity.

An initial, locally unbalanced state will have adjusted to balance when transient gravity–inertia waves have propagated into the far field. In this balanced state, we have

$$2\Omega \sin\phi - \frac{\partial(u \cos\phi)}{a \cos\phi\, \partial\phi} + P\frac{\partial p}{\partial\theta} = 0, \tag{10}$$

$$\left(2\Omega \sin\phi + \frac{u \tan\phi}{a}\right)u + \frac{\partial M}{a\partial\phi} = 0, \tag{11}$$

$$\frac{\partial M}{\partial\theta} = c_p\left(\frac{p}{p_0}\right)^{\kappa}, \tag{12}$$

with boundary conditions $u = 0$ at $\phi = \pm\pi/2$, $p = p_T$ at $\theta = \theta_T$, and $M = c_p\theta(p/p_0)^{\kappa}$ at $\theta = \theta_B$. These three equations, along with the associated boundary conditions, constitute an invertibility principle for u, p, and M in terms of the potential vorticity P and the mean mass distribution $\bar{p}(\theta)$. In other words, given $\bar{p}(\theta)$, if we could use (9) to determine the potential vorticity of the final adjusted state as a function of (ϕ, θ), equations (10)–(12), with the associated boundary conditions, could be solved for the three unknowns $u(\phi, \theta)$, $p(\phi, \theta)$, and $M(\phi, \theta)$.

One of the fields obtained in the solution of the system (10)–(12) is the final adjusted mass distribution $p(\phi, \theta)$. However, a major component of $p(\phi, \theta)$ is the mean mass distribution $\bar{p}(\theta)$, which is known a priori. Thus, it is possible to restate the invertibility problem (10)–(12) in terms of $p'(\phi, \theta) \equiv p(\phi, \theta) - \bar{p}(\theta)$. With this approach it is also convenient to define $M'(\phi, \theta) \equiv M(\phi, \theta) - \bar{M}(\theta)$, where $\bar{M}(\theta)$ is determined from $\partial\bar{M}/\partial\theta = c_p(\bar{p}/p_0)^{\kappa}$ with lower boundary condition $\bar{M} = c_p\theta(\bar{p}/p_0)^{\kappa}$ at $\theta = \theta_B$. It is also convenient to define the potential vorticity anomaly as $P'(\phi, \theta) \equiv P(\phi, \theta) - \bar{P}(\phi, \theta)$, where $\bar{P}(\phi, \theta) = (2\Omega \sin\phi)/\bar{\sigma}$ and $\bar{\sigma} = (-\partial\bar{p}/\partial\theta)$, and to define the potential latitude $\Phi(\phi, \theta)$ by $\Omega a \sin^2\Phi = \Omega a \sin^2\phi - u \cos\phi$ (Schubert et al. 1991). With these definitions and the shorthand notation $S = \sin\Phi$, $s = \sin\phi$, (10)–(12) can be restated as

$$\Omega\frac{\partial(S^2 - s^2)}{\partial s} + \bar{P}\frac{\partial p'}{\partial\theta} = \sigma P', \tag{13}$$

$$\Omega^2 a^2 s\left(2 - \frac{S^2 - s^2}{1 - s^2}\right)\left(\frac{S^2 - s^2}{1 - s^2}\right) = \frac{\partial M'}{\partial s}, \tag{14}$$

$$\frac{\partial M'}{\partial\theta} = c_p\left[\left(\frac{\bar{p} + p'}{p_0}\right)^{\kappa} - \left(\frac{\bar{p}}{p_0}\right)^{\kappa}\right], \tag{15}$$

with boundary conditions $S = 1$ at $s = 1$, $S = -1$ at $s = -1$, $p' = 0$ at $\theta = \theta_T$, and $M' = c_p\theta[((\bar{p} + p')/p_0)^{\kappa} - (\bar{p}/p_0)^{\kappa}]$ at $\theta = \theta_B$. These three equations constitute an invertibility principle for $S(s, \theta)$, $p'(s, \theta)$, and $M'(s, \theta)$ in terms of the potential vorticity anomaly $P'(s, \theta)$. In other words, if we could determine from (9) the potential vorticity anomaly of the final adjusted state as a function of (s, θ), equations (13)–(15), with the associated boundary conditions, could be solved for the three unknowns $S(s, \theta)$, $p'(s, \theta)$, and $M'(s, \theta)$.

There are many other ways to look at the invertibility problem. For example, starting from (10)–(12) and using various elimination procedures, we could also express the invertibility principle in three different ways, that is, as second-order partial differential equations for any of the variables u, p, or M. Alternatively, starting from (13)–(15), we could express the invertibility principle as second-order partial differential equations for S, p', or M'. As an example of one of the many ways to look at the invertibility problem, let us consider the second-order partial differential equation for u. To express the invertibility problem in terms of u, we differentiate (10) with respect to ϕ and use the thermal wind equation to obtain

$$\frac{\partial}{a\partial\phi}\left(\frac{\partial(u \cos\phi)}{a \cos\phi\, \partial\phi}\right) + P\frac{\partial}{\partial\theta}\left(\frac{2\Omega \sin\phi + (2u \tan\phi)/a}{\Gamma}\frac{\partial u}{\partial\theta}\right) = \frac{2\Omega \cos\phi}{a} - \sigma\frac{\partial P}{a\partial\phi}, \tag{16a}$$

where $\Gamma = d\Pi/dp = \kappa\Pi/p$. Expressing the previous boundary conditions in terms of u, we obtain

$$u = 0 \quad \text{at} \quad \phi = \pm\frac{\pi}{2}, \tag{16b}$$

$$\frac{\partial u}{\partial\theta} = 0 \quad \text{at} \quad \theta = \theta_T,$$

$$\frac{\partial u}{\partial\theta} = \left(\frac{2\Omega \sin\phi + (u \tan\phi)/a}{2\Omega \sin\phi + (2u \tan\phi)/a}\right)\frac{u}{\theta_B} \quad \text{at} \quad \theta = \theta_B. \tag{16c}$$

The invertibility problem (16) is the spherical coordinate analog of the f-plane problem studied by Hoskins et al. (1985, p. 901). Note that this invertibility problem is nonlinear but can be linearized by approximating Γ and σ as known reference functions of θ and by neglecting the $u \tan\phi$ terms in the interior equation (16a) and the lower boundary condition (16c).

All the above ways of looking at the adjustment problem suffer from the same complication—the determination of the final potential vorticity field as a

function of (ϕ, θ). The difficulty is that (9) states that P is conserved on fluid particles, so that the determination of the final P field as a function of (ϕ, θ) depends on the complicated advection by the oscillating (due to gravity–inertia wave propagation) v field. This problem can be circumvented by transforming to a new meridional coordinate that converts (9) into a local conservation equation. This procedure, which makes v implicit in the coordinate transformation, is discussed in the next section.

3. Dynamical adjustment problem in the potential latitude coordinate

Because the flow is adiabatic, the material derivative operator (5) is already simplified in the sense that the "vertical advection" term $\dot{\theta}\partial/\partial\theta$ has vanished. To gain an even further simplification of (5), let us consider a transformation of the meridional coordinate. To accomplish this transformation we first note that the zonal momentum equation (1) can also be written in the form $D(\Omega a \sin^2\phi - u\cos\phi)/Dt = 0$, or, using the definition of potential latitude, $D\Phi/Dt = 0$. Let us now consider (Φ, Θ, τ) space, where $\Theta = \theta$ and $\tau = t$. The symbols Θ and τ are introduced to distinguish partial derivatives at fixed ϕ ($\partial/\partial\theta$ and $\partial/\partial\tau$) from partial derivatives at fixed Φ ($\partial/\partial\Theta$ and $\partial/\partial\tau$). We can now easily show that (5) can also be written as

$$\frac{D}{Dt} = \frac{\partial}{\partial\tau}. \tag{17}$$

The advantage of (17) over (5) is the elimination of the divergent wind component v, which is now implicit in the coordinate transformation.

Let us now introduce the potential pseudodensity $\sigma^* = (2\Omega \sin\Phi/\zeta)\sigma$. The potential pseudodensity is related to the potential vorticity by $\sigma^* P = 2\Omega \sin\Phi$ and is simply the pseudodensity a parcel would acquire if ζ were changed to $2\Omega \sin\Phi$ under conservation of P. Since σ^* is proportional to P^{-1}, the potential pseudodensity equation can be easily obtained from the potential vorticity equation (9). Then, with D/Dt given by (17), the potential pseudodensity equation becomes

$$\frac{\partial\sigma^*}{\partial\tau} = 0, \tag{18}$$

so that σ^* is invariant at fixed points in (Φ, Θ) space.

Now that $\sigma^*(S, \Theta)$ has been determined analytically, our final theoretical task is to express the invertibility principle in (S, Θ) space. We first use the definition of σ^* to obtain the Jacobian form $\partial(s, p)/\partial(S, \Theta) + \sigma^* = 0$. We then introduce the Bernoulli function $\mathcal{M} = M + \frac{1}{2}u^2$ and its deviation $\mathcal{M}' = \mathcal{M} - \bar{M}$ and express the balance and hydrostatic relations in terms of $\mathcal{M}'$. The invertibility principle becomes

$$\bar{\sigma}\frac{\partial s}{\partial S} - \frac{\partial(s, p')}{\partial(S, \Theta)} = \sigma^*, \tag{19}$$

$$2\Omega^2 a^2 S\left(\frac{S^2 - s^2}{1 - s^2}\right) = \frac{\partial\mathcal{M}'}{\partial S}, \tag{20}$$

$$\frac{\partial\mathcal{M}'}{\partial\Theta} = c_p\left[\left(\frac{\bar{p} + p'}{p_0}\right)^\kappa - \left(\frac{\bar{p}}{p_0}\right)^\kappa\right], \tag{21}$$

with boundary conditions $s = 1$ at $S = 1$, $s = -1$ at $S = -1$, $p' = 0$ at $\Theta = \Theta_T$, and $\mathcal{M}' = c_p\theta[((\bar{p} + p')/p_0)^\kappa - (\bar{p}/p_0)^\kappa]$ at $\Theta = \Theta_B$.

When comparing the (S, Θ)-space invertibility problem (19)–(21) with the (s, θ)-space invertibility problem (13)–(15), an important difference should be kept in mind. The formulation of the invertibility problem in terms of $\sigma^*(S, \Theta)$ does not require independent specification of $\bar{p}(\theta)$. Rather, the $\sigma^*(S, \Theta)$ field implies an associated $\bar{p}(\theta)$. This is easily seen as follows. Assuming that $p = p_T$ at the model top $\theta = \theta_T$, we can integrate the relation $\sigma = -\partial p/\partial\theta$ to obtain

$$p(\phi, \theta) = p_T + \int_\theta^{\theta_T} \sigma(\phi, \theta')d\theta'. \tag{22}$$

Now the mean pressure on an isentropic surface is

$$\bar{p}(\theta) = \frac{1}{2}\int_{-\pi/2}^{\pi/2} p(\phi, \theta)\cos\phi d\phi. \tag{23}$$

Using (22) in (23) we obtain

$$\bar{p}(\theta) = p_T + \frac{1}{2}\int_\theta^{\theta_T}\int_{-\pi/2}^{\pi/2} \sigma(\phi, \theta')\cos\phi d\phi d\theta'$$

$$= p_T + \frac{1}{2}\int_\Theta^{\Theta_T}\int_{-\pi/2}^{\pi/2} \sigma^*(\Phi, \Theta')\cos\Phi d\Phi d\Theta', \tag{24}$$

where the last step follows from $\cos\phi d\phi d\theta = (2\Omega \sin\Phi/\zeta)\cos\Phi d\Phi d\Theta$ and $\sigma^* = (2\Omega \sin\Phi/\zeta)\sigma$. Thus, when $\sigma^*(\Phi, \Theta)$ is known, an average pressure on each Θ surface is implied.

We can now summarize the results of our analysis as follows. Since the time evolution of the σ^* field is determined from (18), we can then iteratively solve the diagnostic problem (19)–(21) for s, p', and $\mathcal{M}'$, after which u is easily determined. This is all accomplished in (S, Θ) space. The transformation to other representations [e.g., $u(\phi, \theta)$, $u(\phi, p)$, $p(\phi, \theta)$, or $\theta(\phi, p)$] is straightforward.

4. Dynamical adjustment of the trade inversion layer

a. *Experiment 1: Dynamical extension of subtropical inversions into the Tropics*

Using the results of an idealized adjustment problem, we shall now illustrate how sharp inversions in the subtropics can be dynamically extended into the deep Tropics. For this idealized problem let us consider the initial wind field $u = v = 0$. Since there is no initial rotational flow, $\Phi = \phi$ (or equivalently $S = s$) and $\sigma^* = \sigma$ initially. Thus, we conclude from (18) that $\sigma^*(\Phi,$

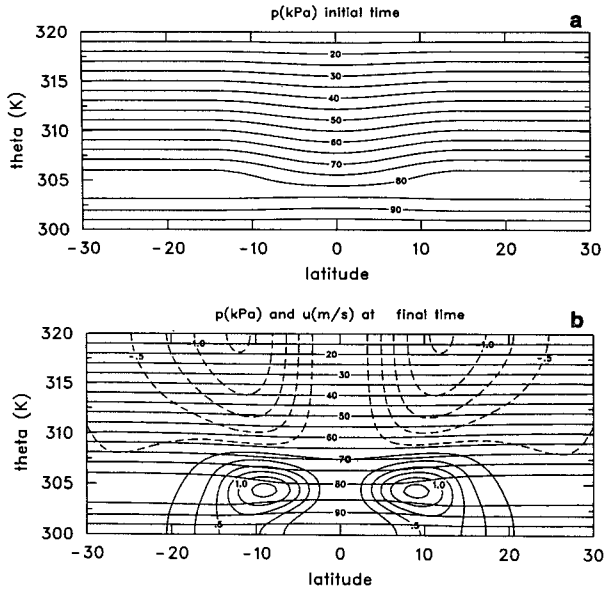

FIG. 8. Results for experiment 1. (a) Isoline of $p(\phi, \theta)$ for the initial unbalanced state. (b) isolines of $p(\phi, \theta)$ and $u(\phi, \theta)$ for the final balanced state. Solid wind contours indicate westerly flow; dashed contours easterly flow, with a contour interval of 0.25 m s^{-1}.

$\Theta, \infty) = \sigma(\phi, \theta, 0)$, which can be substituted into the right-hand side of (19). For the initial mass field we choose

$$\sigma(\phi, \theta, 0) = \sigma_0 + \hat{\sigma}F(\theta)\begin{cases} 1 & \phi_w \leq \phi \leq \pi/2 \\ \frac{1}{2}[1 - \cos(\pi\phi/\phi_w)] & \\ & -\phi_w \leq \phi \leq \phi_w \\ 1 & -\pi/2 \leq \phi \leq -\phi_w, \end{cases} \tag{25}$$

where

$$F(\theta) = -\frac{(\theta_2 - \theta_1)}{2(\theta_T - \theta_B)} + \frac{1}{2}\begin{cases} 0 & \theta_2 \leq \theta \leq \theta_T \\ 1 + \cos[\pi(2\theta - \theta_2 - \theta_1)/(\theta_2 - \theta_1)] & \\ & \theta_1 \leq \theta \leq \theta_2 \\ 0 & \theta_B \leq \theta \leq \theta_1. \end{cases} \tag{26}$$

Note that the vertical integral of (26) from θ_B to θ_T vanishes. The constants appearing in (25) and (26) are specified as follows: $\theta_B = 300$ K, $\theta_T = 320$ K, $\theta_1 = 302$ K, $\theta_2 = 307$ K, $\sigma_0 = 4.5$ kPa K^{-1}, $\hat{\sigma} = -4.4$ kPa K^{-1}, and $\phi_w = \pi/9$. This choice of parameters results in a subtropical inversion layer centered near 825 mb with a maximum stability of $\partial T/\partial z = 1.5$ K km^{-1}.

The $p(\phi, \theta)$ field at the initial state and the $p(\phi, \theta)$ and $u(\phi, \theta)$ fields at the final adjusted state are shown in Fig. 8. The same information on the mass field is displayed in $\theta(\phi, p)$ plots for the initial and final states in Fig. 9. At the initial time there is an inversion layer just below 800 mb in the subtropics but no inversion near the equator. This state is not in dynamic balance, since there is no initial wind but a nonzero initial variation of θ on a p surface (or, equivalently, an initial nonzero variation of p on a θ surface). To reach dynamic equilibrium a westerly flow at the inversion level near the equator is required. The generation of such a westerly flow can be accomplished by the poleward shift of air parcels near 800 mb in the equatorial region. By mass continuity and the adiabatic constraint, such poleward shifts tend to fill in isentropic layers in subtropical latitudes (decreasing the stability there) and evacuate isentropic layers near the equator (increasing the stability there). The end result is the dynamical extension of the subtropical inversion into the tropical region. The subtlety of this process is reflected in the weak zonal winds produced ($\leq$1.3 m s^{-1}) and the small meridional parcel shifts involved. (A 25-km poleward shift produces a 1 m s^{-1} westerly zonal flow at 15°N.) Although the zonal winds and meridional particle shifts are small, the effect on the static stability field is significant—a reflection of the general rule of dynamic adjustment of the mass field to the wind field in the Tropics (e.g., Gill 1982, p. 191). The lapse rates

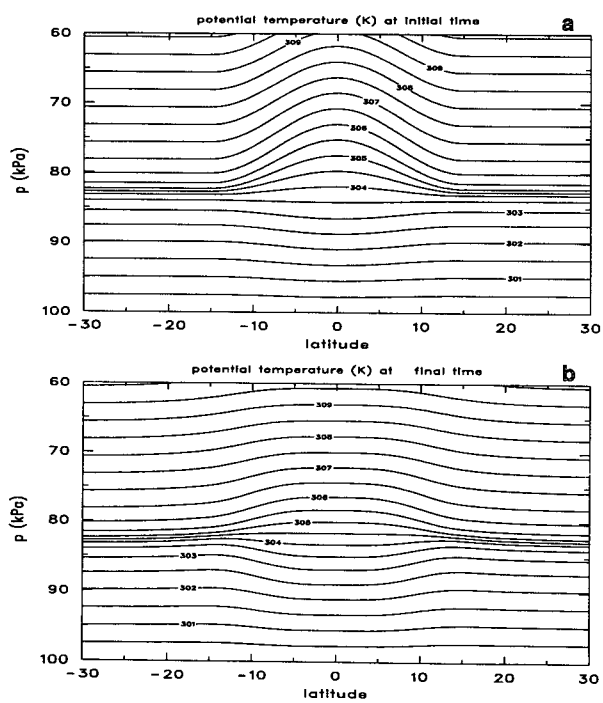

FIG. 9. Results for experiment 1. (a) Isolines of $\theta(\phi, p)$ for the initial unbalanced state. (b) Isolines of $\theta(\phi, p)$ for the final balanced state.

for the initial and final states at the equator and 30° latitude are shown in Fig. 10. The static stability in the inversion at 30° latitude decreases, while a meridionally extended stable layer appears at the equator.

The results presented in Figs. 8–10 are fairly insensitive to the strength of the initial subtropical stable layer. For example, varying the initial strength of the subtropical stable layer over a range from −4 to 5 K km^{-1} has only minor effects on the final adjusted zonal wind and static stability fields, which range from 1 to 1.3 m s^{-1} at 9°N and −6.5 to −6.0 K km^{-1} at the equator, respectively.

It is possible to interpret this idealized experiment in a different sense. Imagine convective and radiative processes that operate to sharpen the inversion at 800 mb in subtropical latitudes but not near the equator. A sequence of slow dynamical adjustments then results in a poleward drift of equatorial air along isentropic surfaces extending into the developing inversion. This tends to weaken the subtropical inversion and strengthen the tropical inversion, with the end result again being a dynamical extension of inversion structure into the deep Tropics.

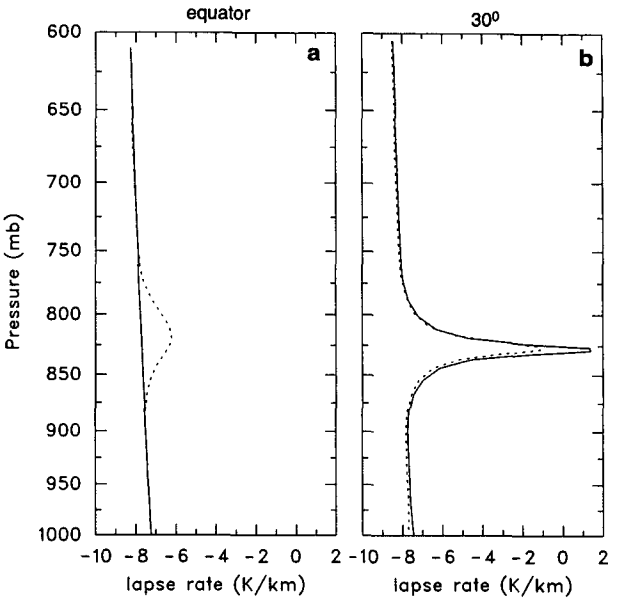

FIG. 10. Lapse rate $\partial T/\partial z$ as a function of pressure for the initial state (solid curves) and the final adjusted state (dashed curves) at the equator (panel a) and at 30° latitude (panel b) for experiment 1. Initially there is a stable layer at 30° latitude but not at the equator. In the final state the stable layer has been dynamically extended to the equator.

b. *Experiment 2: Adjustment of a sloping trade inversion layer*

Let us now consider a second idealized problem that illustrates the dynamical adjustments opposing the formation of sharp, sloping inversions in the Tropics. For this second problem let us also consider the initial condition $u = v = 0$, so that again $\sigma^*(\Phi, \Theta, \infty) = \sigma(\phi, \theta, 0)$. For this case we choose to specify $p(\phi, \theta, 0)$, from which $\sigma(\phi, \theta, 0)$ is easily calculated by differentiation. The initial pressure field is given by

$$p(\phi, \theta, 0) = p_B - \sigma_0(\theta - \theta_B) + \Delta p \begin{cases} 1 & \theta_2(\phi) \le \theta \le \theta_T \\ G\left(\dfrac{\theta - \theta_1}{\theta_2 - \theta_1}\right) & \theta_1(\phi) \le \theta \le \theta_2(\phi) \\ 0 & \theta_B \le \theta \le \theta_1(\phi), \end{cases} \quad (27)$$

where

$$\theta_1(\phi) = 303K = 4K \begin{cases} 0 & \phi_n \le \phi \le \pi/2 \\ G\left(\dfrac{\phi_n - \phi}{\phi_n}\right) & 0 \le \phi \le \phi_n \\ G\left(\dfrac{\phi_s - \phi}{\phi_s}\right) & \phi_s \le \phi \le 0 \\ 0 & -\pi/2 \le \phi \le \phi_s, \end{cases} \quad (28)$$

with $\theta_2(\phi) = \theta_1(\phi) + 3K$ and $G(x) = \exp\{-(\gamma/x)\exp[1/(x-1)]\}$, an interpolating function. Note that $G(0) = 0$, $G(1) = 1$, and with the choice $\gamma = 1/2$ $\exp(2)\ln(2)$, $G(1/2) = 1/2$. The constants appearing in (27) and (28) are specified as follows: $p_B = 100$ kPa, $\theta_B = 300$ K, $\theta_T = 320$ K, $\sigma_0 = 4.5$ kPa K^{-1}, $\Delta p = 5.8$ kPa, $\phi_s = -\pi/8$, and $\phi_n = \pi/8$.

The fields of $\theta(\phi, p)$ at the initial and final states are shown in Fig. 11. The corresponding zonal flows (not shown) are, as in the previous experiment (cf. Fig. 8), easterly above the inversion and westerly below the inversion. The final adjusted zonal winds are again weak, with the maximum values just exceeding 1 m s^{-1}. On the $\theta = 304$ K surface, equatorial air shifts poleward and fills mass into the flat subtropical inversion. In contrast, on the $\theta = 308$ K surface, air shifts equatorward and fills mass into the flat section of the equatorial inversion. On an intermediate surface (e.g., $\theta = 306$ K), air at 20°N and 20°S shifts equatorward, while air at 5°N and 5°S shifts poleward, which fills mass into the sharp sloping inversion. The end result is a significant weakening of the flat section of the equatorial inversion near 650 mb, the formation of an equatorial inversion near 800 mb, and the destruction of the sharpness of the original sloping section of the inversion. Note that it is not the overall slope of the trade inversion that is decreased during adjustment but rather the slope of each isentropic surface. The lapse rates for the initial and final states at the equator and 30°N are shown in Fig. 12. Finally, it is worth noting that the equatorial stable layer is 25 mb higher than the subtropical stable layer, which yields a slope in approximate agreement with observations.

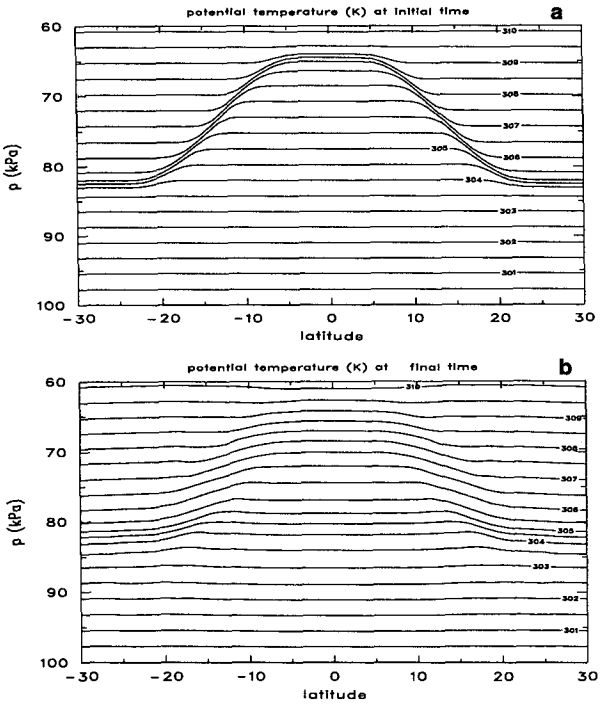

FIG. 11. Results for experiment 2. (a) Isolines of $\theta(\phi, p)$ for the initial unbalanced state. (b) Isolines of $\theta(\phi, p)$ for the final balanced state.

Another physical interpretation of these results is as follows. Attempts by equatorial diabatic processes to reset the inversion to a higher level are opposed, with the result that the higher inversion is weakened and the lower inversion is reestablished. Of course, these results do not imply that it is impossible to form a sharp sloping inversion in the deep Tropics. Rather, they imply that it is difficult or "inefficient" to form sharp sloping inversions because of large-scale dynamical constraints.

5. Concluding remarks

Through the use of a zonally symmetric model we have shown how the trade wind inversion layer can be viewed as a structure that is dynamically constrained to be more horizontally uniform than pure thermodynamical arguments would suggest. The misconception generated by purely thermodynamic models of the horizontally homogeneous type is that the height of the trade inversion is controlled by the *local values* of sea surface temperature, divergence, and atmospheric temperature and moisture above the inversion. The dynamical view brings in the notion that the trade inversion layer is strongly coupled horizontally. Rapid spatial variations in trade inversion height are dynamically smoothed. In this way, the trade inversion height is controlled by horizontally averaged values of the sea surface temperature, divergence, and above-inversion atmospheric structure. The horizontal scale over which this averaging occurs is difficult to characterize in terms of the Rossby length associated with a particular vertical normal mode, because we are usually dealing with vertically thin initial anomalies, which project almost equally onto all the vertical normal modes.

It is sometimes argued that boundary-layer processes can be parameterized in general circulation models in a purely thermodynamic manner, that is, by appending equations that predict the boundary-layer depth and thermodynamic structure. Such arguments should be viewed with caution, because the model may then have more vertical degrees of freedom in the mass field than the wind field. This means that part of the mass field is out of control of the dynamical adjustment process. Effects such as the ones we have discussed in this paper may then be improperly simulated.

Observational studies from the Atlantic, Eastern Pacific, and most recently from the Western Pacific warm pool region reveal that the trade wind boundary layer is a common feature throughout the Tropics, with an associated inversion cap around 800 mb. From these studies, which are summarized in section 1, it is clear that additional research should be conducted with the goal of producing monthly or seasonal distributions of trade wind inversion height over the entire tropical and subtropical regions. New tools such as 915-MHz wind profilers are capable of continuously monitoring the trade inversion (Rogers et al. 1993) and could be used in such future studies.

In closing, we would like to emphasize that we have not presented a complete theory of the trade inversion

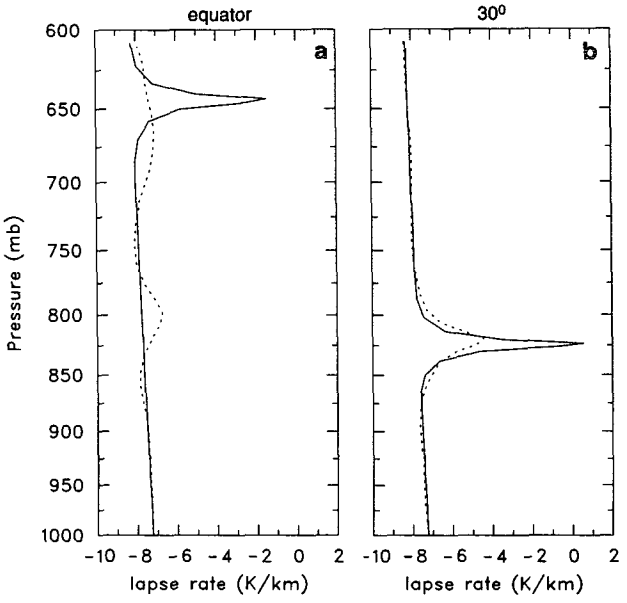

FIG. 12. Lapse rate $\partial T/\partial z$ as a function of pressure for the initial state (solid curves) and the final adjusted state (dashed curves) at the equator (panel a) and at 30° latitude (panel b) for experiment 2.

but rather a simplified argument that isolates one of the dynamical aspects of the problem. Future theoretical and modeling research might involve the construction of complete trade wind boundary layer theories, which can be studied in a pure thermodynamic mode or a coupled dynamic–thermodynamic mode. Comparison of the results from these two modes of model implementation would give better understanding of the basic concept presented here, that is, the concept that dynamical coupling leads to a trade inversion height that is fairly uniform over the tropical and subtropical regions.

Acknowledgments. We wish to thank Scott Hausman for his help with the graphics. This research was supported by the Office of Naval Research under Grant N00014-91-J-1422 and by NOAA through TOGA/COARE Grant NA37RJ0202.

REFERENCES

Albrecht, B. A., 1979: A model for the thermodynamic structure of the trade-wind boundary layer: Part II. Applications. *J. Atmos. Sci.*, **36,** 90–98.

——, 1984: A model study of downstream variations of the thermodynamic structure of the trade winds. *Tellus,* **36A,** 187–202.

——, A. K. Betts, W. H. Schubert, and S. K. Cox, 1979: A model for the thermodynamic structure of the trade-wind boundary layer: Part I. Theoretical formulation and sensitivity tests. *J. Atmos. Sci.,* **36,** 73–89.

Augstein, E., H. Schmidt, and F. Ostapoff, 1974: The vertical structure of the atmospheric planetary boundary layer in undisturbed trade winds over the Atlantic Ocean. *Bound.-Layer Meteor.,* **6,** 129–150.

Betts, A. K., 1973: Nonprecipitating cumulus convection and its parameterization. *Quart. J. Roy. Meteor. Soc.,* **99,** 178–196.

——, and B. A. Albrecht, 1987: Conserved variable analysis of the convective boundary layer thermodynamic structure over the tropical oceans. *J. Atmos. Sci.,* **44,** 83–99.

Bretherton, C. S., 1993: Understanding Albrecht's model of trade cumulus cloud fields. *J. Atmos. Sci.,* **50,** 2264–2283.

Chertock, B., C. W. Fairall, and A. B. White, 1993: Surface-based measurements and satellite retrievals of broken cloud properties in the equatorial Pacific. *J. Geophys. Res.,* **98,** 18 489–18 500.

Firestone, J. K., and B. A. Albrecht, 1986: The structure of the atmospheric boundary layer in the central equatorial Pacific during January and February of FGGE. *Mon. Wea. Rev.,* **114,** 2219–2231.

Gill, A. E., 1982: *Atmosphere–Ocean Dynamics.* Academic Press, 662 pp.

Gutnick, M., 1958: Climatology of the trade-wind inversion in the Caribbean. *Bull. Amer. Meteor. Soc.,* **39,** 410–420.

Hack, J. J., W. H. Schubert, D. E. Stevens, and H.-C. Kuo, 1989: Response of the Hadley circulation to convective forcing in the ITCZ. *J. Atmos. Sci.,* **46,** 2957–2973.

Haraguchi, P. Y., 1968: Inversions over the tropical eastern Pacific Ocean. *Mon. Wea. Rev.,* **96,** 177–185.

Held, I. M., and A. Y. Hou, 1980: Nonlinear axially symmetric circulations in a nearly inviscid atmosphere. *J. Atmos. Sci.,* **37,** 515–533.

Holland, J. Z., and E. M. Rasmusson, 1973: Measurements of the atmospheric mass, energy, and momentum budgets over a 500-kilometer square of tropical ocean. *Mon. Wea. Rev.,* **101,** 44–55.

Hoskins, B. J., M. E. McIntyre, and A. W. Robertson, 1985: On the use and significance of isentropic potential vorticity maps. *Quart. J. Roy. Meteor. Soc.,* **111,** 877–946.

Johnson, R. H., J. F. Bresch, P. E. Ciesielski, and W. A. Gallus, 1993: The TOGA/COARE atmospheric sounding array: Its performance and preliminary scientific results. Preprints, *20th Conf. on Hurricanes and Tropical Meteorology,* San Antonio, TX, Amer. Meteor. Soc., 1–4.

——, P. E. Ciesielski, and K. A. Hart, 1995: Tropical inversions near the 0°C level. *J. Atmos. Sci.,* submitted.

Kloesel, K. A., and B. A. Albrecht, 1989: Low-level inversions over the tropical Pacific—Thermodynamic structure of the boundary layer and the above-inversion moisture structure. *Mon. Wea. Rev.,* **117,** 87–101.

Lilly, D. K., 1968: Models of cloud-topped mixed layers under a strong inversion. *Quart. J. Roy. Meteor. Soc.,* **94,** 292–309.

Nitta, T., and S. Esbensen, 1974: Heat and moisture budget analyses using BOMEX data. *Mon. Wea. Rev.,* **102,** 17–28.

Ramage, C. S., S. J. S. Khalsa, and B. N. Meisner, 1981: The central Pacific near-equatorial convergence zone. *J. Geophys. Res.,* **86,** 6580–6598.

Randall, D. A., 1980: Entrainment into a stratocumulus layer with distributed radiative cooling. *J. Atmos. Sci.,* **37,** 148–159.

Rogers, R. R., W. L. Ecklund, D. A. Carter, K. S. Gage, and S. A. Ethier, 1993: Research applications of a boundary-layer wind profiler. *Bull. Amer. Meteor. Soc.,* **74,** 567–580.

Sarachik, E. S., 1985: A simple theory for the vertical structure of the tropical atmosphere. *Pure Appl. Geophys.,* **123,** 261–271.

Schneider, E. K., 1977: Axially symmetric steady-state models of the basic state for instability and climate studies. Part II: Nonlinear calculations. *J. Atmos. Sci.,* **34,** 280–296.

Schubert, W. H., J. S. Wakefield, E. J. Steiner, and S. K. Cox, 1979a: Marine stratocumulus convection. Part I: Governing equations and horizontally homogeneous solutions. *J. Atmos. Sci.,* **36,** 1286–1307.

——, ——, ——, and ——, 1979b: Marine stratocumulus convection. Part II: Horizontally inhomogeneous solutions. *J. Atmos. Sci.,* **36,** 1308–1324.

——, P. E. Ciesielski, T. B. McKee, J. D. Kleist, S. K. Cox, C. M. Johnson-Pasqua, and W. L. Smith Jr., 1987: Analysis of boundary layer sounding data from the FIRE marine stratocumulus project. Department of Atmospheric Science, Colorado State University, Report 419, 97 pp.

——, ——, D. E. Stevens, and H.-C. Kuo, 1991: Potential vorticity modeling of the ITCZ and the Hadley circulation. *J. Atmos. Sci.,* **48,** 1493–1509.

——, S. K. Cox, T. B. McKee, D. A. Randall, P. E. Ciesielski, J. D. Kleist, and E. L. Stevens, 1992: Analysis of sounding data from Porto Santo Island during ASTEX. Department of Atmospheric Science, Colorado State University, Report 512, 96 pp.

von Ficker, H., 1936: Die passatinversion. *Veroeff. Meteor. Inst. Univ. Berlin,* **1,** 1–33.

Wakefield, J. S., and W. H. Schubert, 1981: Mixed-layer model simulation of Eastern North Pacific stratocumulus. *Mon. Wea. Rev.,* **109,** 1959–1968.